Available online at www.sciencedirect.com
SCIENCE DIRECT
Polymer 47 (2006) 4760–4767
polymer
www.elsevier.com/locate/polymer

Multi-walled carbon nanotubes reinforced nylon 6 composites

Guang-Xin Chen [a,b], Hun-Sik Kim [a], Byung Hyun Park [a], Jin-San Yoon [a,*]

[a] Department of Polymer Science and Engineering, Inha University, Incheon 402-751, South Korea
[b] College of Materials Science and Engineering, Beijing University of Chemical Technology, P.O. Box 206, Beijing 100029, China

Received 21 November 2005; received in revised form 31 March 2006; accepted 16 April 2006
Available online 19 May 2006

Abstract

Multiwalled carbon nanotubes (MWNT) were functionalized with amine groups using a 'grafting to' technique. The oxidized MWNT (MWNT–COOH) were converted to the acyl chloride functionalized MWNT (MWNT–COCl) by treating them with thionyl chloride ($SOCl_2$), and then MWNT–COCl was reacted with hexamethylenediamine to prepare MWNT–NH_2. The formation of MWNT–NH_2 was confirmed through the FTIR observation. MWNT–NH_2/nylon 6 composites with different MWNT loadings were prepared by the simple melt compounding approach. A fine dispersion of MWNTs throughout nylon 6 matrix was observed by SEM and TEM. The fractured surface of the composites showed not only a uniform dispersion of MWNTs but also a strong interfacial adhesion with the matrix, as evidenced by the presence of many broken but strongly embedded MWNTs in the matrix in the absence of debonding of MWNTs from the matrix. Incorporation of MWNTs improved the mechanical properties significantly. Higher thermal stability was obtained for the composites with better dispersed MWNTs.

Keywords: Nylon 6; Multiwalled carbon nanotube; Aamine groups

1. Introduction

Fiber-reinforced polymer composites are used in many structural materials because they show a significant improvement in strength and toughness over the neat polymer. First, from a structural point of view, the fiber spacing should be smaller than the characteristic strength limiting flaw [1], and thus, smaller fiber diameters are desirable in order to produce a higher packing density. Second, a uniform fiber distribution within the matrix is necessary in order to avoid unreinforced regions in the matrix and thereby distribute the load evenly throughout the composite. To ensure efficient load transfer from the matrix to the fiber, the interfacial bonding between the polymer matrix and the fiber must be optimized to prevent the fiber debonding [2]. The covalent bond between the matrix and fiber constitutes the strongest type of interfacial bonding, and it is preferred in the situations where the strength of the reinforcing agent is significantly higher than that of the matrix.

Carbon nanotubes (CNTs) are considered to be the ideal reinforcing agent for high-strength polymer composites because of their tremendous mechanical strength, nanometer-scale diameter, and high aspect ratio [3]. Studies have shown that carbon nanotubes have ca. 1000 GPa of Young's modulus, which is much higher than that of the conventional carbon fibers (200–800 GPa) [4,5]. Despite the advantages of single-walled carbon nanotubes (SWNTs) compared with those of multiwalled ones (MWNTs), a problem associated with the fabrication of polymer composites using SWNTs is that during loading the individual tubes tend to pull out from the ropes (bundles), thus making load transfer difficult. Therefore, the composite reinforcement is dominated by the collective behavior of the bundles rather than by the strength of the individual tubules [6–8]. As far as the MWNTs are concerned, it is noteworthy that MWNTs produced using the arc-discharge method are highly crystalline and defect-free, and the surface is inert so that polymers cannot attach firmly to it. Thus, the introduction of defects via oxidation routes using strong acids or the use of pyrolytically carbon-grown nanotubes (containing defects and kinks) may be an alternative to fabricate composites in which the tube surface is strongly bonded to the polymeric matrix [9]. It has been confirmed that refluxing CNTs with concentrated nitric acid creates acidic sites on CNTs, such as carboxylic, carbonyl, and hydroxyl groups [10–12]. These reactive groups on CNTs greatly enhance the coupling of CNTs with polymer matrix, thus improve the mechanical strength of the nanocomposites [13]. Sidewall functionalization of CNTs with organic chains or functional

* Corresponding author.
E-mail addresses: gxchen@eyou.com (G.-X. Chen), jsyoon@inha.ac.kr (J.-S. Yoon).

0032-3861/$ - see front matter © 2006 Elsevier Ltd. All rights reserved.
doi:10.1016/j.polymer.2006.04.020

groups is another efficient way to improve the dispersion and strengthen the coupling of CNTs with polymer matrix [14,15].

In the past decade, a number of methods have been applied for the synthesis of carbon nanotube–polymer composites: physical mixing of the carbon nanotubes with preformed polymers in solution or in molten state [16–18], electrospinning [19], in situ polymerization in the presence of carbon nanotubes [20,21], surfactant-assisted processing of CNT–polymer composites [22], and chemical modification of the incorporated carbon nanotubes [23,24]. As a result of these studies, impressive progress has been achieved. For example, the direct mixing of multiwalled carbon nanotubes (MWNTs) and polystyrene led to 36–42% increase in elastic stiffness and 25% increase in tensile strength with the incorporation of only 1 wt% of MWNTs into the polystyrene matrix [16]. In situ polymerization of poly(*p*-phenylene benzobisoxazole) (PBO) in the presence of 10 wt% SWNTs led to 50% increase in tensile strength together with reduced shrinkage and high-temperature creep [20]. By using surfactant-assisted dispersion of SWNTs, it was possible to spin fibers from a nanotube–polymer dispersion [22], which yielded fibers of low elastic modulus with exceptionally high flexibility [25]. In the case of functionalized SWNT precursors it was shown that the incorporation of 1 wt% fluorinated and acid-treated SWNTs into an epoxy composite led to 30% increase in Young's modulus and 18% increase in tensile strength [23].

Xia et al. prepared MWNT/nylon 6 composites by microemulsion approach to avoid the impediment of growing polymer chains due to the presence of CNTs [26]. Liu et al. prepared successfully MWNT/nylon 6 nanocomposites by using the simple melt compounding method [27]. Most recently, Haddon et al. [28] obtained CNT–nylon 6 composite fibers by using a chemical processing technology that allowed the continuous spinning of the composites produced from the in situ polymerization of caprolactam in the presence of CNTs.

Most of the MWNTs eventually are debonded at the MWNTs/polymer interface and subsequently pulled out from the polymer matrix rather than broken down, indicating a weak interfacial interaction between the nanotubes and the matrix [29]. Therefore, the improvement in mechanical properties of polymer/MWNT nanocomposites with small amount of the nanotubes is frequently limited due mainly to the formation of severe agglomeration of the nanotubes and/or poor interfacial interaction with the polymer matrix.

In this study, MWNTs functionalized with amine groups were prepared and melt compounded with nylon 6. The morphology and mechanical properties of the resulting composites were explored.

2. Experimental

2.1. Materials

Nylon 6 was purchased from Zigsheng industrial Co. Ltd (Taiwan) with a melt flow index (MFI) of 98 g/min as reported by the manufacturer. The multiwalled carbon nanotubes (MWNTs) were provided by Iljin Nanotech (Korea). The MWNTs were obtained through the chemical vapor deposition method and the purity was higher than 95%.

2.2. Purification of MWNT

The purity of the MWNT was 97%. To remove the impurities such as metallic catalysts in the MWNT, it was treated with 3 M HNO_3 and 1 M H_2SO_4 at 60 °C for 12 h, followed by a reflux process in 5 M HCl at 120 °C for 6 h. The purity of the acid-treated MWNT was measured to be 99% by using the thermogravimetric analysis (TGA, TA Instruments, Q50). These acid-treatments shorten the length of MWNT and introduce carboxyl and hydroxyl groups to MWNT (MWNT–COOH). After the treatment at 400 °C for 3 h to remove the organic molecules, the purified MWNT was obtained.

2.3. Functionalization of MWNT

The acid treated MWNT (MWNT–COOH) was reacted with excess $SOCl_2$ for 24 h under reflux, and then the residual $SOCl_2$ was removed by distillation under a reduced pressure, to yield acyl chloride–functionalized MWNT (MWNT–COCl). The MWNT–COCl was dispersed in chloroform and the mixture was sonicated for 20 min to create a homogeneous suspension. The mixture was added with hexamethylenediamine under nitrogen, and then was immersed in an oil bath at 70 °C under mechanical stirring for 24 h. The resulting reaction medium was vacuum-filtered through a 0.22 μm polycarbonate membrane three times to yield MWNT–NH_2 hybrid.

2.4. Preparation of MWNT/nylon 6 composites

MWNT/nylon 6 composites were prepared by melt compounding of nylon 6 with the MWNTs at 250 °C. The melt compounding was performed by using a Hakke (Rheocord 90) internal mixer at 250 °C for 5 min. The dried pellets were then hot pressed at 250 °C for 1 min under 4 atm to prepare the sheets with a thickness of approximately 0.5 mm to be used for the various characterizations.

2.5. Measurements

Transmission electron microscopy (TEM) images were obtained using a TEM 2000 EX-II microscope (JEOL, Tokyo, Japan) operated at an accelerating voltage of 100 kV to observe the nanoscale structures of the MWNTs and composites. The specimens of MWNTs for the TEM observations were prepared by placing one drop of the sample on a copper grid coated with carbon. All the ultrathin sections of the composites (<100 nm) were microtomed using a Super NOVA 655001 instrument (Leica, Swiss) with a glass knife.

The morphology of the composites was observed with a scanning electron microscope (SEM, Hitachi S-4300) at an accelerating voltage of 15 kV after precoating the sample with a homogenous Pt layer by using an ion sputter (Hitachi, E-1030).

The grafting behavior of the diamine onto the MWNT was monitored by Bio-rad Fourier transformed infrared spectrophotometry (FTIR, Perkin–Elmer, Spectrum 2000, USA).

Thermogravimetric analysis (TGA) was performed with PL-TGA (Polymer Laboratories, Q50, UK) by scanning from 30 to 900 °C at a heating rate of 20 °C/min under nitrogen atmosphere.

Tensile specimens were prepared from the hot pressed sheets. The specimens were subjected to uniaxial elongation at room temperature. All the experiments were carried out with a UTM, Hounsfield test equipment with a cross head speed of 10 mm/min.

3. Results and discussion

Fig. 1 shows FTIR spectra of MWNT–COOH and MWNT–NH_2. Both MWNT–COOH and MWNT–NH_2 show a large band at 3441 cm^{-1} and a weak one at 1634 cm^{-1}, which were attributed, respectively, to the asymmetric bending and scissoring vibrations due to the trace amount of water [30]. In Fig. 1(b), the broad band at 1640 cm^{-1} corresponds to the stretching vibration of the C=O group of the amide functionality. The broad and slightly less intense band at 1540 cm^{-1} was assigned to the combination of the bending vibration of the N–H bond and the stretching vibration of the C–N bond of the amide group. In addition, the intensity of the C–H stretching frequencies at 2853 and 2925 cm^{-1} corresponding to the alkyl groups was more intense in MWNT–NH_2 than that in MWNT–COOH. These FTIR results verify the existence of diamine molecules grafted to the MWNTs through the amide bonds.

The TEM images of MWNT–COOH and MWNT–NH_2 are shown in Fig. 2. It can be seen that the tube surface of MWNT–COOH (Fig. 2(a)) is relatively smooth and clean indicating that the tube was not stained by any impurities. In contrast, MWNT–NH_2 looks stained with an extra phase that was presumed to come mainly from the grafted diamine molecules, as exhibited in Fig. 2(b).

The amount of the grafted diamine molecules was measured to be 5 wt% according to the TGA analysis [31].

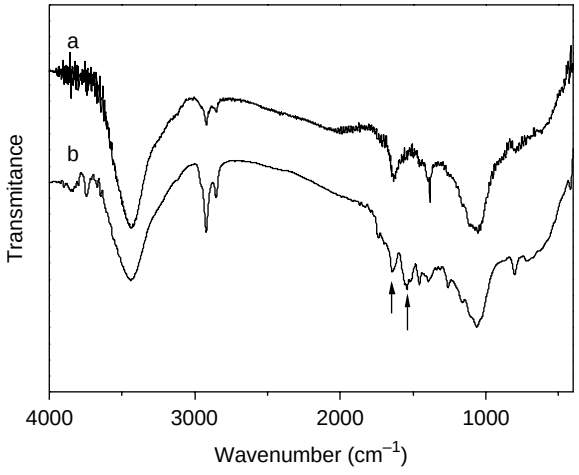

Fig. 1. FTIR spectra of (a) MWNT–COOH, (b) MWNT–NH_2.

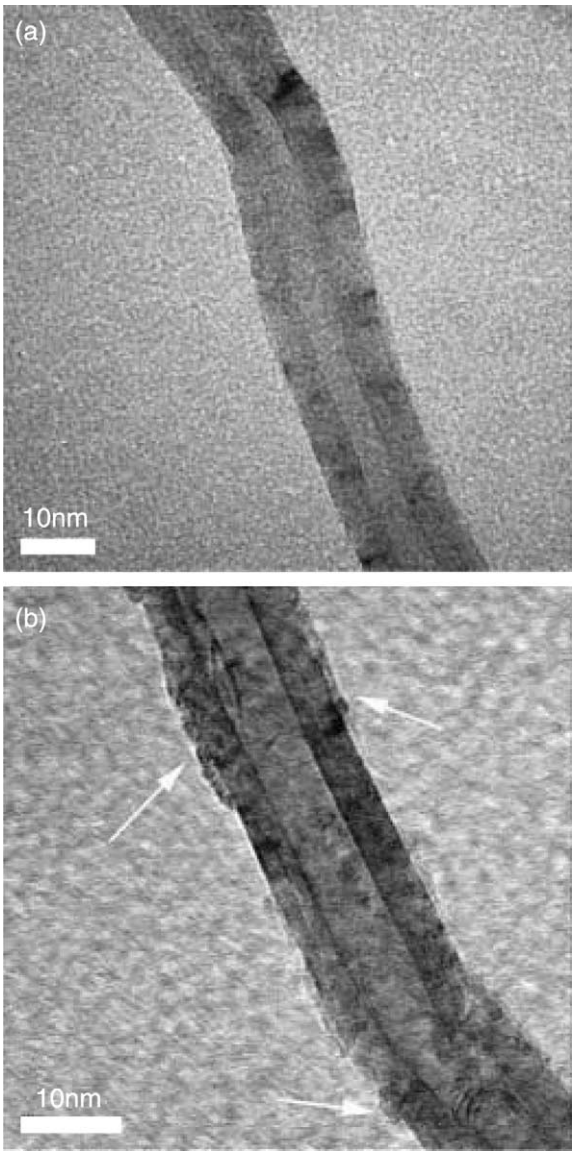

Fig. 2. TEM images of (a) MWNT–COOH, (b) MWNT–NH_2.

The homogeneous dispersion of MWNTs in the polymer matrix is one of the most important requisites for the mechanical strength reinforcement because any inhomogeneities lead eventually to structural defects in the composite material.

Cross-sections of the composites were prepared by fracturing the MWNT/nylon 6 composites in liquid nitrogen to produce an intact fractured surface morphology, and the resulting SEM images are demonstrated in Fig. 3. The bright regions in the SEM images were attributed to MWNTs as a result of their high electrical conductivity. It is unambiguous from Fig. 3 that the MWNT–NH_2 is homogeneously dispersed in the nylon 6 matrix without any aggregation while some aggregates are observed in the MWNT–COOH/nylon 6 composite.

Fig. 4 demonstrates TEM images of the ultrathin section of MWNT–NH_2/nylon 6 composite containing 0.5 wt% of MWNT–NH_2. Fine structure of the MWNTs is observed

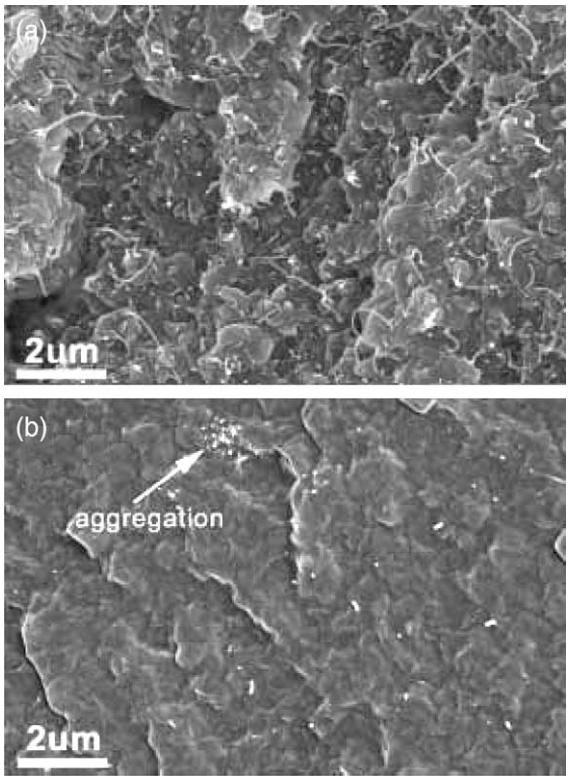

Fig. 3. SEM images of the cross section of the composites fractured at liquid nitrogen temperature for nylon 6 composite containing 0.5 wt% (a) MWNT–NH_2 and (b) MWNT–COOH.

throughout the nylon 6 matrix. The variations in the contrast and the diameter of the MWNTs came mainly from the difference in electron scattering from different depth of the section. As shown in Fig. 4(a), individual nanotubes are randomly dispersed in the matrix. At the same time, most MWNTs are curved in shape due to the flexibility of the nanotubes.

The embedded carbon nanotubes seldom appear as straight inclusions but are rather often characterized by a certain degree of waviness along their axial dimension to reduce the structural reinforcement that the carbon nanotubes would otherwise provide for the host polymer matrix, that is to say the theoretical reinforcement provided by straight inclusion, as pointed out by Fisher et al. [32].

Some nanotubes (Fig. 4(b)) protruding out of the section surface were cut during the ultramicrotoming to allow observation of the cross-section of the nanotube embedded in the matrix. In addition, because of the curved morphology of the nanotubes in the composite, a single nanotube could be cut several times and appear as two or more individual tubes in the TEM image. Clearly, microtoming does not affect the intimate adhesion of the MWNT–NH_2 with the nylon 6 matrix, revealing good wettability between them, as was the case for epoxy/carbon nanotube composites [33].

Typical stress–strain curves of neat nylon 6 and MWNT–NH_2/nylon 6 composites with different MWNT–NH_2 loadings are shown in Fig. 5. Neat nylon 6 exhibits a pronounced yield and post-yield drop, while noticeable yield is hardly detected

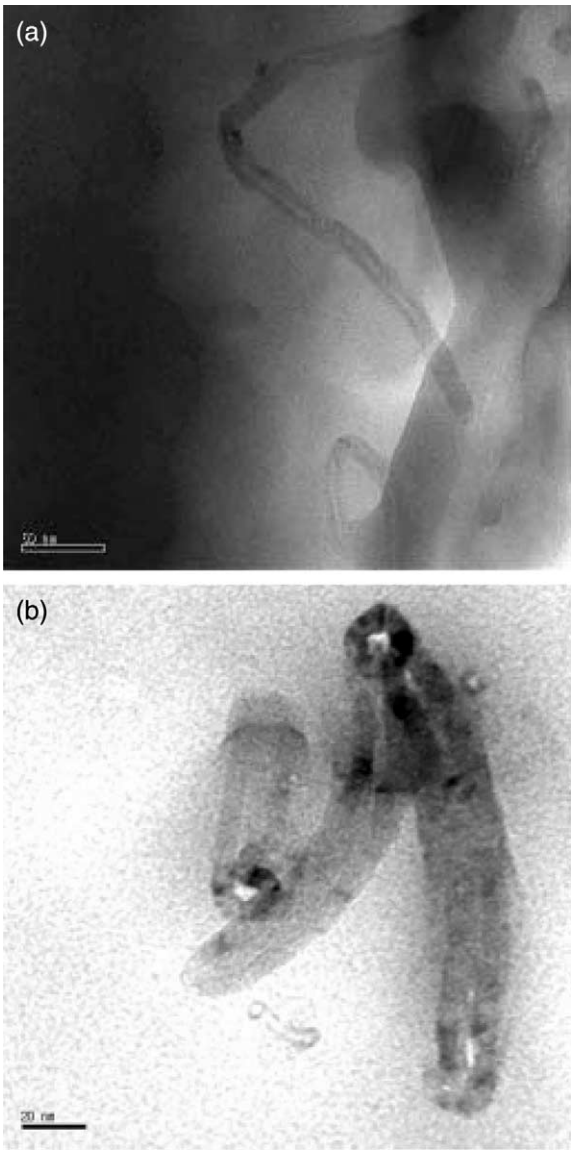

Fig. 4. TEM images showing nanotube dispersion in the ultrathin section of nylon 6 composite containing 0.5 wt% MWNT–NH_2.

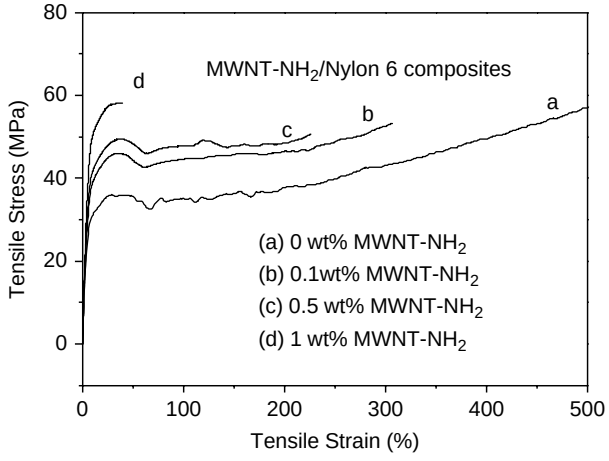

Fig. 5. Stress–strain curves of MWNT–NH_2/nylon 6 composites at different MWNT–NH_2 loadings.

for the MWNT–NH_2/nylon 6 composites as the loading of the nanotube increases. This is probably due to the fact that the MWNTs adhered strongly to the nylon 6 matrix and the sliding of the nylon 6 chains was restricted greatly [28].

Clearly, the incorporation of MWNT–NH_2 into the nylon 6 matrix increased the tensile strength and modulus to make nylon 6 tougher and more resistant to deformation. The tensile test results are summarized in Table 1. The tensile properties of the composites increased with increase in the MWNT–NH_2 loading. Upon incorporation of 2 wt% of MWNTs, the tensile modulus of nylon 6 went up from 1899 to 3556 MPa and the yield strength was enhanced from 35.0 to 59.3 MPa indicating 87 and 69% improvements, respectively. According to the enthalpy of melting, the crystallinity of MWNT–NH_2/nylon 6 composites was slightly lower compared to that of neat nylon 6 (data not shown). Therefore, the increased modulus and strength of the nanotube-containing composites were not attributed to the change in the crystallinity. The possible toughening mechanism will be discussed further by using the SEM observations.

Fig. 6 shows a typical overview on the fissured surface of the composite containing 0.5 wt% of MWNT–NH_2 after the tensile testing. The uniformly dispersed bright dots and lines correspond to the broken MWNTs. The SEM image clearly reveals that an even dispersion of MWNTs was achieved throughout the nylon 6 matrix. Most MWNTs were separated into individual tubes by the shear force during the simple melt compounding and thus evenly dispersed in the matrix, which was of great practical importance for making CNTs reinforced polymer composites. A closer inspection reveals that upon failure most of the MWNTs were broken apart, and some MWNTs were pulled out of the matrix before the breakage. Some loop-like MWNTs are observed with their two ends still strongly embedded in the matrix. This interesting and typical breakage phenomenon of the MWNTs upon the tensile stretching indicates that a strong interfacial adhesion existed between MWNT–NH_2 and nylon 6 matrix and that the load transfer took place efficiently from the matrix to the nanotubes. It is thus believed that the strong interfacial adhesion was responsible for the significant enhancement of the mechanical properties. In contrast, no obvious nanotubes are observed on the fissured surface of MWNT–COOH/nylon 6 composite as shown in Fig. 6(b).

The Halpin-Tsai equation has been used successfully to predict the modulus of polymer/carbon nanotube composites [34,35]. Considering the random distribution of carbon

Table 1
Tensile properties of nylon 6 and MWNT–NH_2/nylon 6 composites

MWNT–NH_2/nylon 6	Modulus (MPa)	Yield strength (MPa)
0/100	1899.2±78.1	35.0±2.9
0.1/99.9	2185.1±142.0	45.8±4.6
0.2/99.8	2290.4±145.6	46.6±4.2
0.5/99.5	2557.7±230.4	49.7±5.4
1/99	3555.5±386.8	59.3±7.0
2/98	3006.3±345.8	54.3±6.9

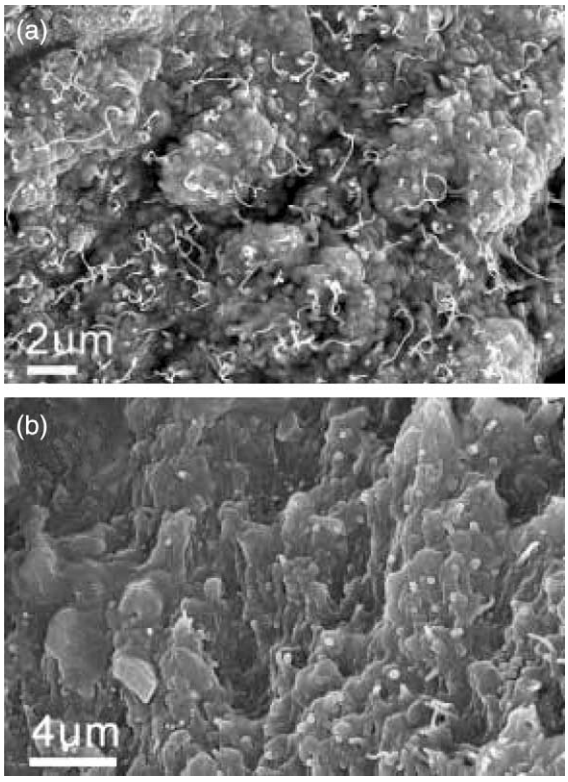

Fig. 6. SEM images showing an overall morphology of failure surface for nylon 6 composite containing 0.5 wt% MWNT–NH_2 (a) and 0.5 wt% of MWNT–COOH (b) after the tensile test.

nanotubes in the polymer matrix, the modified Halpin-Tsai equation can be written as [36,37]:

$$E_C = \left[\frac{3}{8}\frac{1+2(l_{CNT}/D_{CNT})\eta_L V_{CNT}}{1-\eta_L V_{NT}} + \frac{5}{8}\frac{1+2\eta_T V_{CNT}}{1-\eta_T V_{CNT}}\right]E_P \quad (1)$$

$$\eta_L = \frac{E_{CNT}/E_P - 1}{E_{CNT}/E_P + 2l_{CNT}/D_{CNT}} \quad (2)$$

$$\eta_T = \frac{E_{CNT}/E_P - 1}{E_{CNT}/E_P + 2} \quad (3)$$

where E_C, E_{CNT}, and E_P are the tensile modulus of the composite, nanotube, and polymer matrix, respectively. l_{CNT}, D_{CNT}, and V_{CNT} are the length, diameter, and volume fraction of the nanotubes in the composite, respectively. Aspect ratio (l_{CNT}/D_{CNT}) of the reinforcing nanotubes can be estimated if E_C, E_{CNT}, E_P, and V_{CNT} are known.

The modulus of the MWNT–NH_2/nylon 6 composite (E_C) is plotted as a function of the MWNT loading in Fig. 7 setting the density of MWNT–NH_2 to be $\rho = 2.1$ g/cm^3. The average length, l_{CNT}, and diameter of the MWNT, D_{CNT}, were taken to be $l_{CNT} = 2.0$ μm and $D_{CNT} = 0$ nm, respectively. The value of E_{CNT} was assumed to be 1280 GPa.

Fig. 7 shows that the experimentally measured Young's modulus of the composite. Some discrepancies are observed between the theoretically predicted values and the

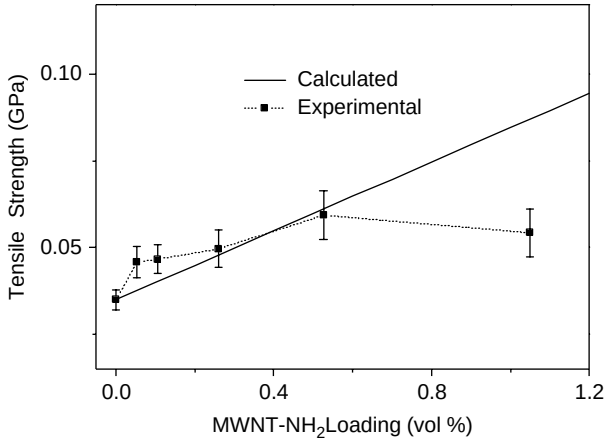

Fig. 7. Young's modulus calculated from the Halpin-Tsai equation under the assumptions: (a) MWNT–NH_2s randomly distributed as a three-dimension network in the composites, and (b) experimental values of the Young's modulus.

experimentally obtained data, which exhibited a maximum Young's modulus at 0.5 wt% of MWNT–NH_2 loading. The tensile strength of the composite can be estimated as [38]:

$$\sigma_C = \sigma_{CNT} V_{CNT} + \sigma_P V_P \quad (4)$$

where σ_C, σ_{CNT}, and σ_P are the tensile strength of the composite, carbon nanotube, and polymer matrix, respectively. The results are summarized in Fig. 8. Again, the experimentally measured tensile strength was higher than that of the theoretically estimated value at low MWNT loading, while the inverse was true at high MWNT loading, indicating that the interfacial interaction was more effective in strengthening the material at low MWNT loading than at high MWNT loading.

Therefore, the assumption that the MWNTs were randomly dispersed in the composites was valid only at low MWNT loading. The well dispersion of the MWNTs at low MWNT loading was presumed to come from the fact that the strong interaction between MWNT–NH_2 and nylon 6 chains, and the high melt viscosity of the composite hindered the orientation of the MWNTs in the matrix. [28] However, a far more intensive melting mixing equipment would be required to prepare the composites with homogeneous dispersion of the MWNTs at high MWNT loading.

Thermogravimetric analysis was performed for the composites, where the weight loss due to the volatilization of the degradation products was monitored as a function of temperature as shown in Fig. 9. It can be seen that the thermal degradation temperature rose slightly as a result of the compounding with the MWNT–NH_2 even though the nanotube content was as low as 0.5 wt%.

It has been known that MWNTs have extremely high thermal conductivity [39,40]. Improvement of interfacial interaction between MWNT and the polymer matrix raises the overall thermal conductivity of the composite, and thus enhances its thermal stability [41]. The more uniform the dispersion of MWNTs, the higher the thermal conductivity of the composite, and in turn the higher the thermal stability.

The thermal degradation of the MWNT–COOH/nylon 6 composites with 0.5 wt% of MWNT was examined for comparison, and their TGA profiles are given in Fig. 9. Admitting the temperature at the maximum mass loss rate in the TGA curve to be an index of thermal stability, the MWNT–COOH/nylon 6 exhibited poorer thermal stability than both neat nylon 6 and MWNT–NH_2/nylon 6 composite, demonstrating that incorporation of MWNTs did not always increase the thermal stability of the composite. Incorporation of MWNTs raised the overall thermal conductivity and thus enhanced the thermal stability of the composites but at the same time the trace amount of water in the MWNTs accelerated the hydrolysis of nylon 6 to lower, in turn, the thermal stability. The FTIR spectra in Fig. 1 confirm the presence of water in the MWNTs. Hydrolysis of amide bond in the nylon 6 chains would not be negligible at the elevated temperature even in the presence of the trace amount of water. The thermal stability results mentioned above were determined by the two competing factors.

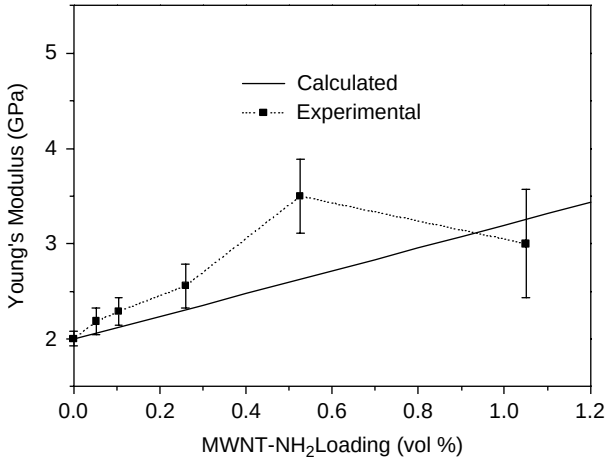

Fig. 8. Tensile strength as a function of MWNT–NH_2 loading: (a) calculated using Eq. (5), and (b) experimentally observed values.

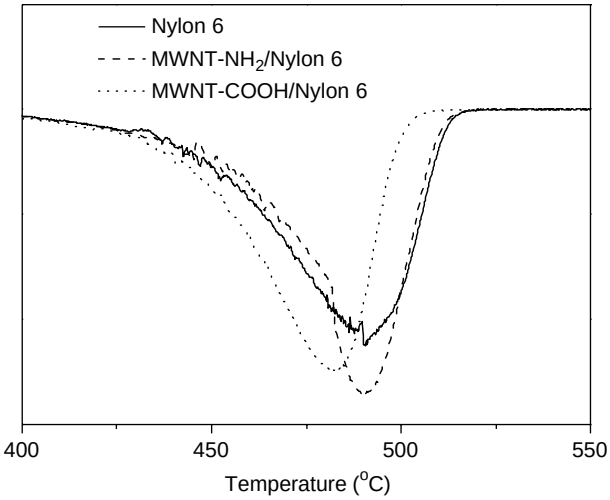

Fig. 9. Thermal decomposition temperature of nylon 6 and MWNTs/nylon 6 composites with 0.5 wt% nanotubes.

The higher thermal stability of MWNT–NH_2/nylon 6 than that of MWNT–COOH/nylon 6 again reveals the well dispersion of MWNT–NH_2 owing to the strong interfacial interaction.

Activation energy for the thermal decomposition, E_t, of the MWNTs/nylon 6 composites with 0.5 wt% MWNTs can be estimated from the corresponding TGA curves by using the integral method proposed by Horowitz and Metzger [42]

$$\ln[\ln(1-\alpha)^{-1}] = \frac{E_t\theta}{RT_{max}^2} \quad (5)$$

where α is the decomposed fraction, and E_t is the activation energy of decomposition. T_{max} is the temperature at maximum rate of weight loss, and θ is $(T-T_{max})$. R is the gas constant. From the plots of $\ln[\ln(1-\alpha)^{-1}]$ vs θ, which are exemplified in Fig. 10, the activation energy (E_t) can be determined from the slope of the straight line of the plots. E_t of MWNT–NH_2/nylon 6 composite was 317 kJ/mol while E_t of MWNT–COOH/nylon 6 composite was 295 kJ/mol. The higher E_t of MWNT–NH_2/nylon 6 than that of MWNT–COOH/nylon 6 discloses that the former composite with more uniform dispersion of MWNTs was more thermally stable than the latter composite with aggregated MWNTs.

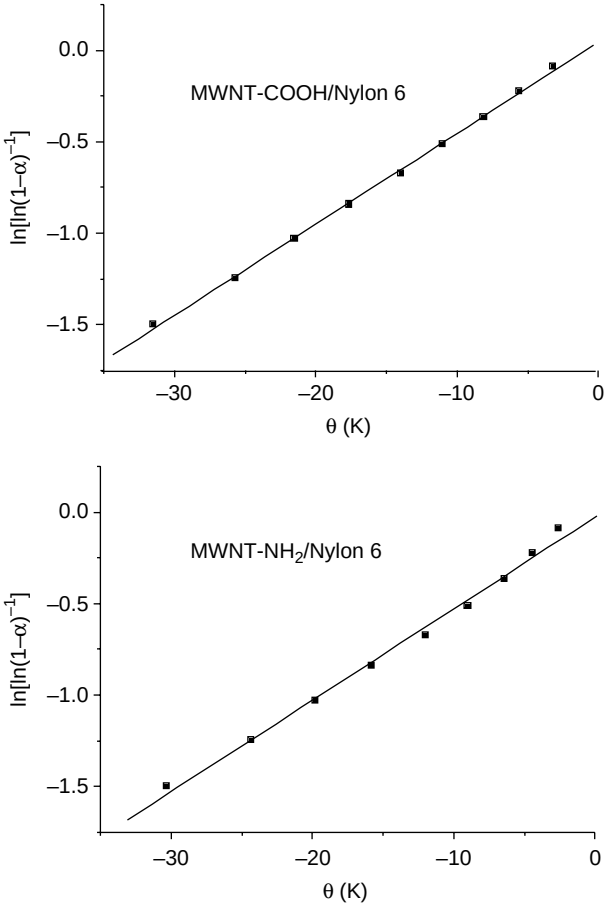

Fig. 10. Plots of $\ln[\ln(1-\alpha)-1]$ vs θ for determination of the decomposition activation energy of MWNTs/nylon with 0.5 wt% nanotubes. Straight line is the linear fit of the data points.

4. Conclusions

Multiwalled carbon nanotubes were functionalized successfully with hexamethylenediamine. The resulting MWNT–NH_2 reinforced nylon 6 composites efficiently through a simple melt compounding to endow them with excellent mechanical properties. The possible reaction between carboxyl end groups of nylon 6 and –NH_2 groups and the surface roughness of the MWNT–NH_2 enhanced the MWNT–nylon 6 interfacial interaction and improved their compatibility, and this allowed a homogeneous dispersion of the MWNTs in the nylon 6 matrix. The Young's modulus and tensile strength of nylon 6 were greatly improved by the incorporation of MWNTs via the current process. Microscopic observations revealed that a more uniform and fine dispersion of MWNTs were achieved throughout the nylon 6 matrix after the functionalization due to the stronger interfacial adhesion between the nanotubes and the matrix. Thermal stability of the composites was higher and thus higher value of activation energy of thermal degradation was obtained for the composites with better dispersed MWNTs.

Acknowledgements

Authors are gratefully acknowledging the financial support by Agency for Defence Development, Korea.

References

[1] Chawla KK. Composite materials science and engineering. New York: Springer; 1987.
[2] Peebles LH. Carbon fibers: formation, structure and properties. Boca Raton, Fl: CRC Press; 1995.
[3] Calvert P. Nature 1999;399:210.
[4] Salvetat JP, Briggs GAD, Bonard JM, Basca RR, Kulik AJ, Stockli T, et al. Phys Rev Lett 1999;82:944.
[5] Yu MF, Files BS, Arepalli S, Ruoff RS. Phys Rev Lett 2000;84:5552.
[6] Ajayan PM, Schadler LS, Giannaris C, Rubio A. Adv Mater 2000;12:750.
[7] Barrera EV. J Miner Metall Mater Soc 2000;52A:38.
[8] McCarthy B, Coleman JN, Czerw R, Dalton AB, Panhuis MIH, Maiti A, et al. J Phys Chem B 2002;106:2210.
[9] Terrones M. Annu Rev Mater Res 2003;33:419.
[10] Satishkumar BC, Govindaraj A, Mofokeng J, Subbanna GN, Rao CNR. J Phys D: Appl Phys 1996;29:4925.
[11] Kuznetsova A, Mawhinney DB, Naumenko V, Yates Jr JT, Liu J, Smalley RE. Chem Phys Lett; 2000;321:292.
[12] Ebbsen TW, Hiura H, Bischer ME. Adv Mater 1996;8:155.
[13] Jang J, Bae J, Yoon SH. J Mater Chem 2003;13:676.
[14] Mitchell CA, Bahr JL, Arepalli S, Tour JM, Krishnamoorti R. Macromolecules 2002;35:8825.
[15] Lin Y, Hill DE, Bentley J, Allard LF, Sun YP. J Phys Chem B 2003;107:10453.
[16] Qian D, Dickey EC, Andrews R, Rantell T. Appl Phys Lett 2000;76:2868.
[17] Steuerman DW, Star A, Narizzano R, Choi H, Ries RS, Nicolini C, et al. J Phys Chem B 2002;106:3124.
[18] Meincke O, Kaempfer D, Weickmann H, Friedrich C, Vathauer M, Warth H. Polymer 2004;45:739.
[19] Sen R, Zhao B, Perea DE, Itkis ME, Hu H, Love J, et al. Nano Lett 2004;4:459.
[20] Kumar S, Dang TD, Arnold FE, Bhattacharyya AR, Min BG, Zhang X, et al. Macromolecules 2002;35:9039.

[21] Deng J, Ding X, Zhang W, Peng Y, Wang J, Long X, et al. Eur Polym J 2002;38:2497.
[22] Vigolo B, Poulin P, Lucas M, Launois P, Bernier P. Appl Phys Lett 2002; 81:1210.
[23] Zhu J, Kim J, Peng H, Margrave JL, Khabashesku VN, Barrera EV. Nano Lett 2003;3:1107.
[24] Chen GX, Kim HS, Park BH, Yoon JS. J Phys Chem B 2005;109:22237.
[25] Salvetat JP, Briggs GAD, Bonard JM, Basca RR, Kulik AJ, Stockli T, et al. Phys Rev Lett 1999;82:944.
[26] Xia H, Wang Q, Qiu G. Chem Mater 2003;15:3879.
[27] Zhang WD, Shen L, Phang IY, Liu TX. Macromolecules 2004;37:256.
[28] Gao J, Itkis ME, Yu A, Bekyarova E, Zhao B, Haddon RC. J Am Chem Soc 2005;127:3847.
[29] Qian D, Dickey EC. J Microsc 2001;204:39.
[30] Yao Z, Braidy N, Botton GA, Adronov A. J Am Chem Soc 2003;125: 16015.
[31] Chen GX, Kim HS, Park BH, Yoon JS. J Polym Sci, Part B. Submitted for publication.
[32] Fisher FT, Bradshaw RD, Brinson LC. Appl Phys Lett 2002;80:4647.
[33] Ajayan PM, Stephan O, Colliex C, Trauth D. Science 1994;265:1212.
[34] Qian D, Dickey EC, Andrews R, Rantell T. Appl Phys Lett 2000;76: 2868.
[35] Cadek M, Coleman JN, Barron V, Hedicke K, Blau WJ. Appl Phys Lett 2002;81:5123.
[36] Mallick PK. In: Fiber-reinforced composites. New York: Marcel Dekker; 1993. p. 91–130.
[37] Zhang X, Liu T, Sreekumar TV, Kumar S, Moore VC, Hauge RH, et al. Nano Lett 2003;9:1285.
[38] Agarwal BD, Broutman LG. Analysis and performance of fiber composites. New York: Wiley; 1980.
[39] Benedict LX, Louie SG, Cohen ML. Solid State Commun 1996;100: 177.
[40] Berber S, Kwon YK, Tomanek D. Phys Rev Lett 2000;84:4614.
[41] Huxtable ST, Cahill DG, Shenogin S, Xue L, Ozisik R, Barone P, et al. Nat Mater 2003;2:731.
[42] Horowitz HH, Metzger G. Anal Chem 1963;35:1464.